Retinotopic remapping of the visual system in deaf adults

Alexandra T. Levine[1,2], Kate Yuen[3], André Gouws[2], Alex R. Wade[1,2,4], Antony B. Morland[1,2,4], Charlotte Codina[5], David Buckley[5], Heidi A. Baseler[1,3,4] *

[1]Department of Psychology,
University of York,
York YO10 5DD, UK

[2]York Neuroimaging Centre,
University of York,
York YO10 5DD, UK

[3]Experimental Medicine and Biomedicine,
Hull York Medical School,
York YO10 5DD, UK

[4]York Biomedical Research Institute,
University of York,
York YO10 5DD, UK

[5]Division of Ophthalmology & Orthoptics,
Health Sciences School,
University of Sheffield,
Sheffield S10 2RX, UK

*Correspondence should be addressed to:

Dr. Heidi A. Baseler
heidi.baseler@york.ac.uk
Phone: +44 1904 322862

Alternative contact:

Dr. Alexandra T. Levine
alexandra.levine@york.ac.uk
Phone: +1 2262197860

Summary

Sound is a vital cue in helping hearing people orient their gaze and attention towards events outside their central line of sight, especially in the far periphery, where vision is poor. Without sound cues, deaf individuals must rely on vision as an 'early warning system' for peripheral events, and in fact numerous behavioural studies demonstrate that deaf adults have superior visual sensitivity [1,2], particularly to far peripheral stimuli [3-5]. We asked whether an increased demand on peripheral vision throughout development might be reflected in early visual brain structures. Using functional magnetic resonance imaging (fMRI), we mapped visual field representations in 16 early, profoundly deaf adults and 16 hearing age-matched controls. To target the far periphery, we used wide-field retinotopic mapping stimuli to map visual field eccentricity out to 72°, well beyond conventional mapping studies [6-10]. Deaf individuals exhibited a larger representation of the far peripheral visual field in both the primary visual cortex and the lateral geniculate nucleus of the thalamus. Importantly, this was not due to a total expansion of the visual map, as there was no difference between groups in overall size of either structure, but a smaller representation of the central visual field in the deaf group, suggesting a redistribution of neural resources. Here, we demonstrate for the first time that the demands placed on vision due to lifelong hearing loss can sculpt visual maps at the first level of inputs from the retina, increasing neural resources for processing stimuli in the far peripheral visual field.

Results

Our aim was to investigate possible neural mechanisms underpinning enhanced peripheral visual sensitivity in deaf adults within early visual processing regions in the brain. As visual processing advantages in deaf individuals are especially prominent in the far periphery [3-5], we compared

eccentricity representations between groups (hearing=16, deaf=16), modifying standard visual mapping methods to include previously unmapped regions in the far periphery. Wide-field retinotopic mapping stimuli were used to identify primary visual cortex (V1) and map visual field eccentricity out to 72° (Fig. 1a). V1 was divided into three equal-sized sub-regions of interest – central (0-15°); mid-peripheral (15-39°) and far-peripheral (39-72°) (Fig. 1a; see methods for more details). Left and right lateral geniculate nuclei (LGN), the main post-retinal visual relay structures in the thalamus, were identified anatomically in each participant using structural (proton density) images (Fig. 1b).

V1 Cortical Volume

First, we compared the total cortical volume of primary visual cortex. We found no difference between deaf and hearing groups (Fig. 2a) ($t(28.19)= -0.154$, $p = .878$), in agreement with a previous study that compared overall size of V1 between deaf and hearing adults within a smaller, more central visual field representation (+/-30°) [11]. Next, we compared the relative volume of the three visual field representations in V1 between deaf and hearing groups, using proportional volume to correct for individual differences in overall V1 size. A mixed factorial analysis of variance (ANOVA) revealed a significant interaction between sub-region and group ($F(1,30)= 7.608$, $p = .002$, $\eta2= .923$), indicating that volume is distributed differently across the three visual field representations between deaf and hearing groups (Fig. 2b). Between-group comparisons indicated a significantly larger central representation in hearing participants ($t(23.22) = 2.98$, $p = .007$), no significant difference in the mid-peripheral representation ($t(26.83) = -0.452$, $p = .655$), and a significantly larger far-peripheral representation in deaf participants ($t(24.93) = -2.62$, $p = .015$: Fig. 2b).

V1 Cortical Thickness

As differences in cortical volume can be affected either by changes in cortical thickness or surface area (or both), we compared both measures separately between groups. We found no difference in overall mean cortical thickness (all of V1) between deaf and hearing groups (ANOVA; Group, $F(1,30) = .037$, $p = .849$, $\eta 2 = .054$; see Fig. 2d). There was a significant difference in thickness between eccentricity representations across both groups (Region, $F(1.589,47.674) = 14.145$, $p < .001$, $\eta 2 = .992$), reflecting well-known thickness differences in between the occipital pole (representing the central visual field and the calcarine sulcus (representing the periphery present in all human brains). Importantly, however, there was no significant interaction between region and group, suggesting cortical thickness does not account for the group differences in volume found above (Region*Group: $F(1.589,47.674)= .923$, $p = .384$, $\eta 2= .183$).

V1 Cortical Surface Area

Cortical surface area of each eccentricity representation was compared next, again using relative proportions to correct for individual differences in overall V1 surface area (Fig. 2c). An ANOVA revealed a significant interaction between sub-region and group ($F(1,30)= 7.608$, $p = .002$, $\eta 2= .923$), as seen in the volume measure. Between-group comparisons indicated a significantly larger central representation in hearing participants ($t(21.53) = 2.93$, $p = .008$, $d = .10$), no significant difference in the mid-peripheral representation ($t(27.42) = -0.244$, $p = .809$, $d = .08$), and a significantly larger far-peripheral representation in deaf participants ($t(25.97) = -2.50$, $p = .019$, $d= .91$: Fig. 2c). This suggests that volumetric differences between groups reflected changes in surface area rather than cortical thickness.

Cortical Magnification in V1

The distribution of neural resources allocated to processing different visual field locations is conventionally expressed as the areal cortical magnification function (cortical area per unit visual field area), which decreases exponentially with eccentricity in V1 [9]. To estimate cortical magnification functions in V1, we calculated the cortical area per unit visual field area represented by each eccentricity region in each participant. Logarithmic values were plotted as a function of eccentricity to linearize functions, and fit with a linear regression line to estimate gradients (see methods for details). Gradients were significantly shallower in deaf than hearing groups ($t(23.56) = -2.96$, $p = .007$, $d = 2.67$), illustrating a bias towards larger far peripheral representations at the expense of smaller central representations in primary visual cortex in deaf relative to hearing individuals (Fig. 2e).

Visual Field Representations in the Lateral Geniculate Nucleus

Next, we asked whether the redistribution of visual field resources in deaf participants was unique to visual cortex. Previous evidence that projections from peripheral retina are thicker in deaf than hearing adults suggests that cortical differences might be inherited from an earlier stage in the visual pathway [12]. If so, a peripheral bias in visual field representations might also be detectable in the lateral geniculate nucleus (LGN), the thalamic relay structure that receives inputs from the retina and is the main source of projections to V1. To examine this, LGN voxels from each participant were binned according to their preferred eccentricity (stimulus eccentricity producing the maximal functional response). Cumulative histograms were plotted as a function of eccentricity for each group (Fig. 2f). Distributions were significantly different between groups (two-sample Kolmogorov-Smirnov test, $D = 0.094$, $p < 0.001$). The median was significantly higher in the deaf group (18.25°) compared to the hearing group (16.23°). Both groups were positively skewed, with the hearing group exhibiting a more positive skew (1.62), indicating a greater preference towards lower (more central) eccentricities compared to the deaf group (skew

= 1.44). Overall, the LGN data indicate a response bias towards the peripheral visual field in the deaf group relative to the hearing group. This suggests that the redistribution of visual field representations found in primary visual cortex may be inherited in part from earlier structures, such as the LGN.

Discussion

Our results provide the first evidence of compensatory plasticity in the LGN and V1 as a consequence of lifelong auditory deprivation. We reveal a redistribution of neural resources in early deaf individuals, with a larger cortical surface representation of the periphery (>39°), at a cost of smaller representations of the central visual field (<15°). This central/peripheral trade-off in neural resources may explain behavioural differences reported between deaf and hearing individuals. Enhanced peripheral visual sensitivity is reported in deaf cats [3] and adult humans [1,2,13], particularly in the far peripheral visual field [4,5]. Although many studies show no perceptual differences within the central visual field between deaf and hearing adults [1,14], evidence of a central/peripheral trade-off has been reported in deaf adults for some tasks [15,16,17].

Previous studies (and unpublished data from our own group) have revealed differences in visually evoked cortical potentials between deaf and hearing groups, suggesting potential neural substrates for enhanced visual sensitivity [2,18-22]. Further studies using brain imaging and animal models have provided extensive evidence that deaf individuals recruit auditory regions of the brain in response to visual stimuli (crossmodal plasticity) [3,23-27]. Other studies revealed neural differences in deaf individuals in the visual system, but only in higher-order visual areas, such as V5/hMT+ and parietal cortex [28,29]. Within primary sensory cortex, expanded representations of intact inputs have been demonstrated in other populations with sensory loss,

e.g., amputees [30] and those with early partial sight loss [31,32]. In deaf adults, structural changes as early in the visual pathways as the retina have been correlated with enhanced far peripheral sensitivity, leading to the possibility that early visual structures downstream may also be affected [12]. However, previous studies evaluating early visual cortex have found either no difference between deaf and hearing groups [11] or have reported thinner visual cortex and larger population receptive field sizes [33]. Critically, however, these studies were confined to comparisons within a limited visual field (< 37.5°), rather than the far periphery where differences in visual sensitivity are most pronounced and potentially beneficial [4,5].

Most of our deaf participants were fluent in and frequent users of British Sign Language for communication, leading to the possibility that visual experience through signing might contribute to the neural changes observed. Although we observed the same pattern of central/peripheral differences between deaf and hearing groups in both hemispheres, they were most pronounced in the left hemisphere. A left hemisphere bias in deaf individuals has also been reported in visual motion brain regions [29], and may underpin the right visual field (left hemisphere) advantage reported in deaf and hearing signers [4,16,20], compared to hearing non-signers. However, sign language perception is primarily confined within the central/mid-peripheral visual field rather than the far periphery. Moreover, previous studies comparing deaf and hearing native sign language users suggest that plastic changes are primarily due to sensory deprivation, with only modest or no changes with sign language use [1,4,16,26].

Differences in neural resources within the LGN and V1 may partly reflect upstream differences in projections from the retina. Codina and colleagues reported that the retinal nerve fibre layer containing ganglion cell axons from peripheral retina was thicker in deaf participants, while the region containing central projections was thicker in hearing participants [12]. These differences

can lead to changes in downstream projection areas. Our measurements in the LGN suggest that the redistribution of cortical representations is at least in part mediated by feedforward connections. Animal studies in the somatosensory system indicate that thalamic projections can influence cortical plasticity further along the processing pathway [34]. Moreover, differences in the visual field distribution of electrophysiological responses from the retina and cortex in deaf and hearing groups suggest that additional modifications may occur at the level of the cortex (unpublished data). Given the crossmodal recruitment of auditory cortex in deaf individuals, another possibility is that changes in the peripheral representation in V1 might reflect increased input via direct connections from auditory and superior temporal regions to calcarine cortex [35,36].

Until now, remapping in primary visual cortex has only been found when the visual system itself is compromised by disease or dysfunction [31,32]. Our current finding indicates that the sculpting of early visual maps during development can be driven by the demands that are placed on vision due to lifelong hearing loss, even in the absence of any visual deficit. The developmental plasticity of the brain therefore allows it to be tuned by, and probably optimised to, visual behaviour.

Acknowledgements

The authors would like to thank Shradha Billawa, Laura Bridge, Sally Clausen, Eleanor Cole, Vera Wang, Shanelle Canavan, Lucy Spencer, Charlotte Campbell for their contributions in data collection, and the staff at The York Neuroimaging Centre for all their support during this project. Furthermore, we would like to thank Dr Mark Hymers and Dr Edward Silson for useful discussion of the study.

Author contributions

A.T.L.: conceptualization (equal), methodology (equal), software (lead), formal analysis (lead), writing of original draft (lead), visualization (lead). **K.Y:** formal analysis (supporting), writing - review and editing (supporting). **A.D.G.:** methodology (supporting), formal analysis (supporting). **A.R.W.:** methodology (supporting), formal analysis (supporting), supervision (supporting). **A.B.M.:** conceptualization (equal), resources (equal), supervision (supporting). **C.C., D.B.:** writing - review and editing (supporting), resources (supporting). **H.A.B.:** conceptualization (lead), methodology (equal), writing - review and editing (lead), resources (lead), supervision (lead), funding acquisition (lead), project administration (lead), visualization (equal).

Competing Interests statement

The authors declare no competing financial interests.

Figures

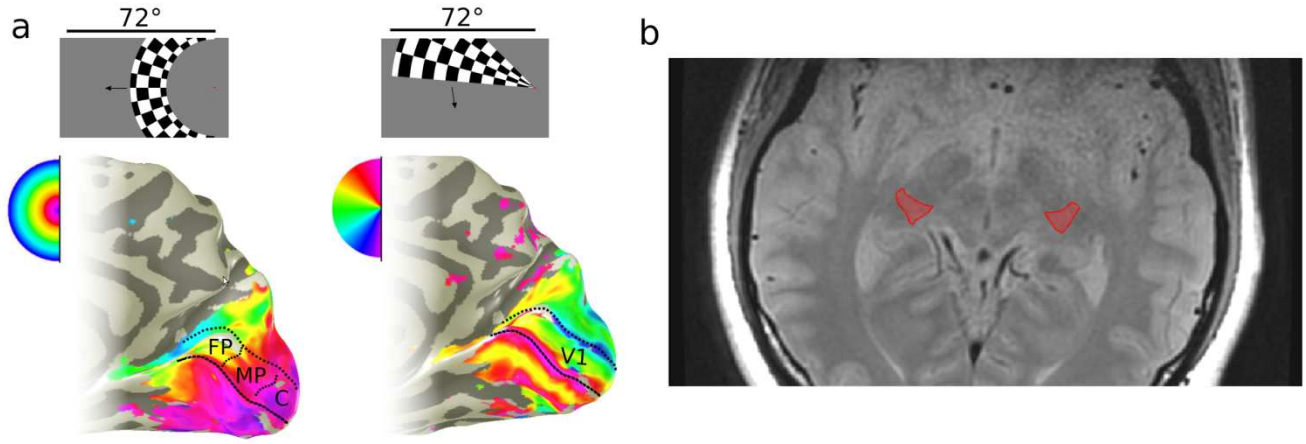

Figure 1. Definition of regions of interest in primary visual cortex (V1) and the lateral geniculate nucleus (LGN). (a) Retinotopic mapping in primary visual cortex (V1). Visual fMRI response maps to expanding ring stimulus (left), and rotating wedge stimulus (right) superimposed on the medial surface of an individual inflated right occipital lobe. Example stimuli shown above. Semicircular key indicates the stimulus position in the visual field maximally activating each part of visual cortex, in false colour. Three regions of interest in V1 marked schematically on left image representing the central (C, 0-15°); mid-peripheral (MP, 15-39°), and far peripheral (FP, 39-72°) visual field. (b) Single axial slice of a proton density scan in one participant. Left and right lateral geniculate nuclei (LGN) are indicated in this slice in red.

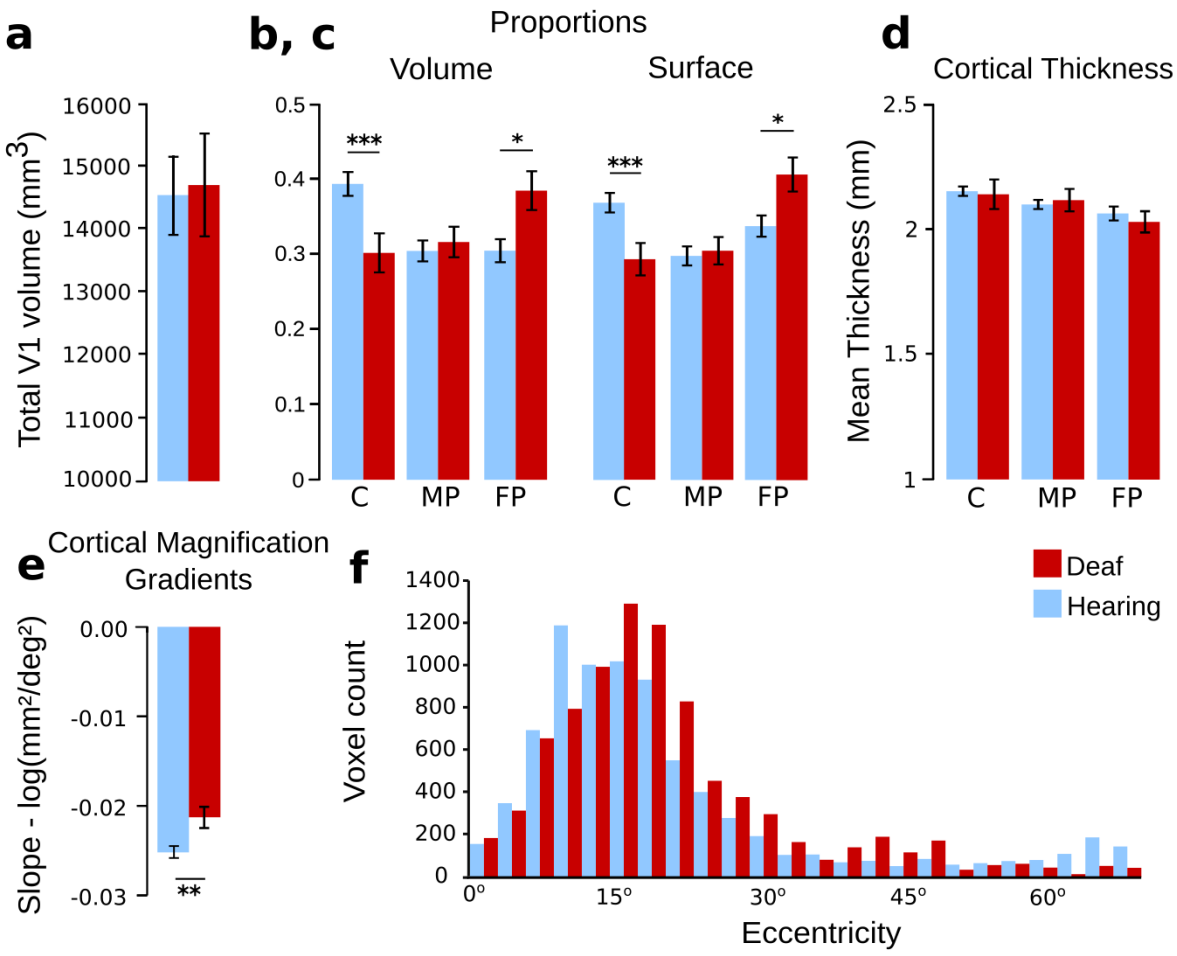

Figure 2. V1 and LGN measurements. V1 total cortical volume, mean cortical thickness, proportion of volume and surface area in V1, cortical magnification gradients and LGN voxel responsiveness to the expanding ring stimulus. (a) Mean total V1 cortical volume based on wide field retinotopic mapping. Mean cortical volume (b) and cortical surface (c) proportions in V1 sub-regions. (d) Mean cortical thickness of V1 areas, grouped by representation of visual field eccentricity. (e) Mean cortical magnification gradients of V1. (e) Preferred eccentricity for voxels in the lateral geniculate nucleus (LGN). Sub-regions represent the central (C, 0-15°); mid-peripheral (MP, 15-39°), and far peripheral (FP, 39-72°) visual field. Error bars represent the mean ± SEM ***p<0.001, **p<0.01, *p<0.05.

STAR+METHODS KEY

RESOURCES TABLE

REAGENT or RESOURCE	SOURCE	IDENTIFIER
Software and Algorithms		
MATLAB (version R2012a)	MathWorks, Natick, MA	https://www.mathworks.com
MrVista (version 3)	Vistalab, Stanford	https://github.com/vistalab/vistasoft
FSL (version 5.0.9)	FMRIB [37]	https://fsl.fmrib.ox.ac.uk/fsl/fslwiki
Psykinematix (version 1.4)	[38]	http://psykinematix.kybervision.net/
FreeSurfer (version 5.3)	[39]	http://surfer.nmr.mgh.harvard.edu/
ITK-Snap (version 2.2.0)	[40]	http://www.itksnap.org/pmwiki/pmwiki.php
R	[41]	https://www.r-project.org/
SPSS (version 20)	SPSS (IBM SPSS Statistics 20)	https://www.ibm.com/analytics/spss-statistics-software

CONTACT FOR REAGENT AND RESOURCE SHARING

Further information and requests for resources should be directed to the Lead Contact, Dr Heidi Baseler.

EXPERIMENTAL MODEL AND SUBJECT DETAILS

The study included 32 participants: 16 early deaf individuals (mean age=34.13, range=20-48 years, 5 females) and 16 hearing individuals (mean age=29.61, range=20-48 years, 5 females). There was no significant difference in age between the groups ($t(30)=1.291$, $p=.207$). All participants had normal or corrected-to-normal vision and gave informed consent in accordance with the Declaration of Helsinki. A British Sign Language (BSL) interpreter was present throughout the sessions for BSL-speaking deaf participants to ensure they understood the instructions and purpose of the study and to answer any questions. Each deaf participant also filled out a brief questionnaire regarding the known aetiology of deafness (Table 1). All deaf participants reported severe to profound hearing loss in both ears (>70db) since infancy (<3 years). The study was approved by The York Neuroimaging Centre Research Governance

Committee.

Table 1. Details of all deaf participants included in the current study.

Subject	Age (at testing)	Gender	Handedness	1st Language	BSL	Cause of hearing loss	Age of onset
1	43	M	Right	English	Yes	Hereditary	Birth
2	48	M	Left	BSL	Yes	In utero measles	Birth
3	47	M	Right	English	Yes	Hereditary	Birth
4	46	M	Right	English	Yes	Rubella	Birth
5	40	M	Right	English	Yes	Sensorineural loss	Birth
6	20	F	Right	English	No	Unknown	2-4 years
7	20	F	Left	English	Yes	Unknown	Unknown
8	48	F	Right	English	Yes	Unknown	Unknown
9	23	F	Right	English	Yes	Sensorineural loss	Birth
10	31	M	Left	BSL	Yes	Hereditary	Birth
11	31	M	Right	English	Yes	Unknown	Birth
12	33	F	Left	BSL	Yes	Unknown	Unknown
13	39	M	Right	BSL	Yes	In utero measles	Birth
14	20	M	Right	BSL	Yes	Hereditary	Birth
15	37	M	Right	English	No	Birth defect	Birth
16	20	M	Left	English	No	Unknown	Birth

METHOD DETAILS

MRI Methods

MRI data were acquired using a 16-channel posterior brain array coil (Nova Medical) in a GE 3 Tesla Signa Excite HD scanner at the York Neuroimaging Centre. High-resolution structural data of the entire brain were acquired with high resolution T1-weighted isotropic scans, (TR, 8 ms; TE, 3 ms; flip angle, 12°; matrix size, 256x256; FOV, 256mm; 176 slices; slice thickness, 1mm; voxel size, 1x1x1mm^3). Structural proton density scans (TR, 2.7s; TE, 36ms; flip angle, 90°; matrix size, 512x512; FOV, 192mm; 39 slices; slice thickness, 2mm; voxel size, 0.37x0.37mm^3) were also acquired prior to and in the same plane as each functional session in order to aid the co-registration of functional data with structural volumes, and identify the lateral geniculate nucleus . Functional data were acquired with a BOLD T2* EPI sequence (TR, 3s; TE, 30ms; flip

angle 90°; matrix size, 128x128; FOV, 192mm; 39 slices; slice thickness, 2mm; voxel size, 1.5x1.5x2mm^3). Each participant underwent one high resolution structural scan, and two sessions consisting of a structural proton density scan followed by functional runs mapping the visual field (one expanding ring, one rotating wedge), testing each hemifield separately.

T1-weighted images were corrected for magnetic spatial inhomogeneities with FMRIB's Automated Segmentation Tool (FAST; [37]). A T2* gradient echo scan was acquired in a subset of participants (3 hearing, 4 deaf), which was used to aid further in inhomogeneity correction. These data were then processed with the FreeSurfer 5.3 analysis suite to segment and reconstruct the grey matter surface [39]. The occipital lobe of the reconstructed image was then corrected by manually segmenting and topology checking in ITK-Snap [40]. These segmentations were used to create flattened cortical representations [42] on which the retinotopic data were displayed using the mrVista toolbox written in Matlab [10].

Retinotopic mapping

Stimulus generation and delivery

Visual maps that included the far peripheral representation were extracted using phase-encoded retinotopic mapping [6-10]. Within this study, two variations of retinotopic stimuli were used. The first version was carried out during pilot scanning of five deaf and four hearing participants. The remaining deaf participants and hearing controls were scanned with a second version of retinotopic stimulus where the parameters of both versions were very closely matched.

The retinotopic stimuli used first were generated with Matlab (version R2012a; The MathWorks, Natick, MA) and presented with MatVis (Neurometrics Institute), and the second version of stimuli were generated either with Psykinematix 1.4 [38] on a Mac Mini OS X and projected to participants through the scanner bore first with a Dukane 8942 ImagePro, then a PROPixx DLP LED projector. These included wedge and ring stimuli, both containing high contrast reversing

checker boards (100% luminance contrast, mean luminance, 98 cd/m^2). The rotating wedge stimulus comprised 30° of a full circle, and extended horizontally to 72° visual angle in each hemifield, vertically ca. +/- 20° visual angle from fixation (Fig. 1a). The Matlab-generated wedge stimulus stepped in 11.25° polar angle increments, and reversed in contrast at 6 Hz, beginning at the upper vertical meridian within both hemifield conditions. The Psykinematix wedge stimulus stepped in 15° increments and contrast reversed at a rate of 4 Hz, beginning at the upper vertical meridian for the right hemifield, and at the lower vertical meridian in the left hemifield. The expanding annulus in both stimulus sets had a total annular width of 14°, and expanded in increments of 4.65° (one check width). As the rings approached the edge of the stimulated field, each ring was replaced by a new one originating from the centre of fixation. A fixation cross, a grey '+' sign, 0.87° in size or a red '+' sign, 0.6° in size, was present throughout the entire scan.

Participants viewed the stimuli at a distance of 275 mm from a supine position through a wide mirror mounted on the head coil, allowing them to see the projection on a custom in-bore acrylic screen (3050mm x 2030mm) mounted behind the head coil. For the Dukane projector, the average luminance of the display was 97.87 cd/m^2 measured with a Minolta Luminance Meter (LS -100/LS 110) and mean luminance of 98.6 cd/m^2 (min-max luminance 2.42-199.7 cd/m^2) for the ProPIXX projector, measured with a Spyder 3 Pro calibration device. The head of each subject was stabilised with foam pads placed inside the head coil and a forehead Velcro-strap to reduce motion artifacts. To increase the restricted field of view normally imposed by the MRI scanner, each hemifield was tested in separate functional scans allowing the stimulus to extend to 72° along the horizontal meridian. Participants viewed stimuli passively, continuously fixating a small cross placed either on the left or right side of the screen depending on which hemifield was being tested. Except in the first sessions (4 hearing, 5 deaf), the head was tilted slightly (ca. 3°)

towards the fixation cross to maximise participant comfort, field of view and fixation and head stability. Instructions were communicated in the MRI scanner between scans, verbally to hearing participants and visually via PowerPoint slides to deaf participants. The deaf participants were asked to push down a button when a message appeared on the screen, and release it when they had read the message and were happy to proceed, and hearing subjects responded verbally. Every participant was provided with an emergency buzzer, which could be pressed at any instance, if they wished to quit the scanning procedure.

MRI data pre-processing

Phase-encoded retinotopic scans were processed with the mrVista toolbox. In order to correct for motion, the T2* functional volumes were aligned to the first acquired volume of the session. Data was slice time corrected and high-pass filtered to remove baseline drifts. MrVista corrects for motion within and between functional volumes and uses a mutual information motion correction algorithm [43]. The corrected functional scans were co-registered to the coordinate space of the high-resolution structural image for each participant using FMRIBs Linear Image Registration Tool (FLIRT; [44]) and the Nestares alignment code [43], which is part of the mrVista toolbox. To aid data visualisation, the phase-encoded retinotopic data were displayed on a flattened representation of the occipital cortex in order to identify boundaries of primary visual cortex (V1) [42]. As the flattening process distorts the distance and area measurements within the 2D dimensions, all coordinates were transformed into the 3D cortical manifold and measurements extracted thereafter [9].

ROI definition

V1 and subdivisions

The delineation of the boundaries of primary visual cortex, V1, was based on previous literature, establishing the identifying features of visual areas [6-10]. In addition, three sub-ROIs were

selected corresponding to the representations of central (0-15°), mid-peripheral (15-39°) and far-peripheral visual field (39-72°). These ranges were defined so each sub-ROI would comprise roughly the same number of voxels, due to cortical magnification. Eccentricity data were displayed on flattened cortex, restricted to the response phase window corresponding to the eccentricity ranges for each sub-ROI. This guided the manual selection of all cortical voxels within each sub-region, not just those voxels which were active. Cortical volume (mm^3), surface area (mm^2) and grey matter thickness (mm) were extracted for each sub-ROI. The surface area measurements were made on the 3D cortical manifold, following the method used by Dougherty and colleagues [9]. In this method, the visual areas are outlined on a 2D flat map, then transformed into the 3D manifold. The surface area was calculated by taking the coordinates belonging to the selected ROI and finding the nearest node on the 3D manifold describing the boundary of grey and white matter.

Lateral Geniculate Nucleus

The left and right lateral geniculate nuclei were identified in each participant using high resolution proton density scans taken in the same slice orientation and location as functional scans (see MRI protocol section) for optimum visualisation of subcortical structures (Fig 1.b) [45-47]. Regions of interest were identified on anonymized scans (K.Y.) and checked by a second individual (H.A.B.) such that the identifier was unaware of whether scans belonged to deaf or hearing participants. Functional voxels falling within the region of interest were analysed from expanding ring scans as with cortical voxels (FFT analysis, phase yields preferred retinal eccentricity for each voxel). A coherence threshold of > 0.23 (uncorrected $p<0.01$) was applied to exclude noisy voxels. As the LGN is small, each participant only contributed a few voxels; therefore, voxels were accumulated across all participants within each group. Group histograms were plotted in 3° eccentricity bins based on the *histcount* function in Matlab, which picks

optimal bin size based on the number and distribution of values. As distributions were skewed towards lower eccentricities, data were log transformed to normalise distributions before statistical evaluation.

QUANTIFICATION AND STATISTICAL ANALYSIS

All the measures described above were tested statistically with R [41] and SPSS (IBM SPSS Statistics 20). All t-tests described in the work were Welch two sample t-tests. Before conducting the general comparison of total V1 volume, a normal distribution confirmed by Shapiro-Wilk test ($W= 0.9792$, $p = 0.776$).

Cortical magnification estimates

The areal cortical magnification was estimated in V1 by dividing the cortical surface area for each ROI (central, mid-peripheral and far peripheral) by the area of visual field represented ($mm^2/degrees^2$). As the areal cortical magnification function typically follows an inverse exponential [9], values were log transformed ($log(mm^2/degrees^2)$) and fit with a linear regression. For each participant, linear fit gradients were calculated for left and right V1, then averaged across hemispheres and then averaged across participants for each group. This provided a metric that is not influenced by individual differences in visual area size [48].

DATA AND SOFTWARE AVAILABILITY

The data that support the findings of this study and the analysis code are available from the Lead Contact upon request.

References

1. Bavelier, D., Dye, M.W.G., and Hauser, P.C. (2006). Do deaf individuals see better? Trends in Cognitive Sciences *10*, 512–518.

2. Pavani, F., and Bottari, D. (2012). Visual abilities in individuals with profound deafness: A critical review. In: The neural bases of multisensory processes. CRC Press/Taylor & Francis.

3. Lomber, S.G., Meredith, M.A., and Kral, A. (2010). Cross-modal plasticity in specific auditory cortices underlies visual compensations in the deaf. Nature Neuroscience *13*, 1421–1427.

4. Codina, C.J., Pascalis, O., Baseler, H.A., Levine, A.T., and Buckley, D. (2016). Peripheral reaction time is faster in deaf adults and British Sign Language interpreters than in hearing adults. Frontiers in Psychology *8*, 1–10.

5. Buckley, D., Codina, C., Bhardwaj, P., and Pascalis, O. (2010). Action video game players and deaf observers have larger Goldmann visual fields. Vision research *50*, 548–556.

6. Sereno, M.I., Dale, A.M., Reppas, J.B., Kwong, K.K., Belliveau, J.W., Brady, T.J., Rosen, B.R., and Tootell, R.B. (1995). Borders of multiple visual areas in humans revealed by functional magnetic resonance imaging. Science (New York, N.Y.) *268*, 889–893.

7. DeYoe, E.A., Carman, G.J., Bandettini, P., Glickman, S., Wieser, J., Cox, R., Miller, D., and Neitz, J. (1996). Mapping striate and extrastriate visual areas in human cerebral cortex. Proceedings of the National Academy of Sciences of the United States of America *93*, 2382–2386.

8. Engel, S.A., Glover, G.H., and Wandell, B.A. (1997). Retinotopic organization in human visual cortex and the spatial precision of functional MRI. Cerebral Cortex *7*, 181–192.

9. Dougherty, R.F., Koch, V.M., Brewer, A.A., Fischer, B., Modersitzki, J., and Wandell, B.A. (2003). Visual field representations and locations of visual areas V1/2/3 in human visual cortex. Journal of Vision *3*, 586–598.

10. Wandell, B.A., Dumoulin, S.O., and Brewer, A.A. (2007). Visual field maps in human cortex. Neuron *56*, 366–383.

11. Fine, I., Finney, E.M., Boynton, G.M., and Dobkins, K.R. (2005). Comparing the effects of auditory deprivation and sign language within the auditory and visual cortex. Journal of Cognitive Neuroscience *17*, 1621–1637.

12. Codina, C., Pascalis, O., Mody, C., Toomey, P., Rose, J., Gummer, L., and Buckley, D. (2011). Visual advantage in deaf adults linked to retinal changes. PLoS ONE *6*, e20417.

13. Loke, W.H., and Song, S. (1991). Central and peripheral visual processing in hearing and nonhearing individuals. Bull. Psychon. Soc., 29:437-440

14. Finney, E.M., and Dobkins, K.R. (2001). Visual contrast sensitivity in deaf versus hearing populations: Exploring the perceptual consequences of auditory deprivation and experience with a visual language. Cognitive Brain Research *11*, 171–183.

15. Proksch, J., and Bavelier, D. (2001). Changes in the spatial distribution of visual attention after early deafness. Journal of Cognitive Neuroscience *14*, 687–701.

16. Bosworth, R.G., and Dobkins, K.R. (2002). Visual field asymmetries for motion processing in deaf and hearing signers. Brain and Cognition 49, 170-181.

17. Samar, V.J., and Berger, L. (2017). Does a flatter general gradient of visual attention explain peripheral advantages and central deficits in deaf adults? Frontiers in Psychology *8*, 713.

18. Neville H.J, Schmidt A, Kutas M. (1983). Altered visual-evoked potentials in congenitally deaf adults. Brain Research. 1983;266(1):127–132.

19. Neville, H., and Lawson, D. (1987a). Attention to central and peripheral visual space in a movement detection task: an event-related potential and behavioral study. I. Normal hearing adults. Brain Research *405*, 253–267.

20. Neville, H., and Lawson, D. (1987b). Attention to central and peripheral visual space in a movement detection task: an event-related potential and behavioral study. II. Congenitally deaf adults. Brain Research 405, 268-83.

21. Bottari, D., Heimler, B., Caclin, A., Dalmolin, A., Giard, M.H., and Pavani, F. (2014). Visual change detection recruits auditory cortices in early deafness. NeuroImage *94*, 172–184.

22. Hauthal, N., Thorne, J.D., Debener, S., Sandmann, P. (2014). Source localisation of visual evoked potentials in congenitally deaf individuals. Brain Topography 27, 412–424

23. Finney EM, Fine I, Dobkins KR. (2001). Visual stimuli activate auditory cortex in the deaf. Nature Neuroscience 4:1171-3.

24. Almeida, J., He, D., Chen, Q., Mahon, B.Z., Zhang, F., Gonçalves, Ó.F., Fang, F., and Bi, Y. (2015). Decoding visual location from neural patterns in the auditory cortex of the congenitally deaf. Psychological Science *26*, 1771–1782

25. Shiell, M.M., and Zatorre, R.J. (2016). White matter structure in the right planum temporale region correlates with visual motion detection thresholds in deaf people. Hearing Research *343*, 6–13.

26. Cardin, V., Smittenaar, R.C., Orfanidou, E., Ronnberg, J., Capek, C.M., Rudner, M., and Woll, B. (2016). Differential activity in Heschl's gyrus between deaf and hearing individuals is due to auditory deprivation rather than language modality. NeuroImage *124*, 96–106.

27. Szwed, M., Bola, Ł., and Zimmermann, M. (2017). Whether the hearing brain hears it or the deaf brain sees it, it's just the same. Proceedings of the National Academy of Sciences *114*, 201710492.

28. Bavelier, D., Tomann, A., Hutton, C., Mitchell, T., Corina, D., Liu, G., and Neville, H. (2000). Visual attention to the periphery is enhanced in congenitally deaf individuals. The Journal of Neuroscience: The official journal of the Society for Neuroscience *20*, RC93.

29. Bavelier D, Brozinsky C, Tomann A, Mitchell T, Neville H, Liu G. (2001). Impact of early deafness and early exposure to sign language on the cerebral organization for motion processing. Journal of Neuroscience 21(22):8931-42. doi: 10.1523/JNEUROSCI.21-22-08931.2001.

30. Ramachandran, V.S., and Rogers-Ramachandran, D. (2000). Phantom limbs and neural plasticity. Archives of Neurology *57*, 317–320.

31. Baseler, H.A., Brewer, A.A., Sharpe, L.T., Morland, A.B., Jägle, H., and Wandell, B.A. (2002). Reorganization of human cortical maps caused by inherited photoreceptor abnormalities. Nature Neuroscience *5*, 364–370.

32. Conner, I.P., Odom, J.V., Schwartz, T.L., and Mendola, J.D. (2007). Retinotopic maps and foveal suppression in the visual cortex of amblyopic adults. Journal of Physiology *583*, 159–173.

33. Smittenaar, C.R., MacSweeney, M., Sereno, M.I., and Schwarzkopf, D.S. (2016). Does congenital deafness affect the structural and functional architecture of primary visual cortex? The Open Neuroimaging Journal *10*, 1–19.

34. Jain, N., Qi, H.X., Collins, C.E., and Kaas, J.H. (2008). Large-scale reorganization in the somatosensory cortex and thalamus after sensory loss in macaque monkeys. Journal of Neuroscience *28*, 11042–11060.

35. Rockland, K.S., and Ojima, H. (2003). Multisensory convergence in calcarine visual areas in macaque monkey. International Journal of Psychophysiology *50*, 19–26.

36. Beer, A.L., Plank, T., and Greenlee, M.W. (2011). Diffusion tensor imaging shows white matter tracts between human auditory and visual cortex. Experimental Brain Research *213*, 299–308.

37. Jenkinson, M., Beckmann, C.F., Behrens, T.E.J., Woolrich, M.W., and Smith, S.M. (2012). FSL. NeuroImage *62*, 782–790.

38. Beaudot, W.H.A. (2009) Psykinematix: a new psychophysical tool for investigating visual impairment due to neural dysfunctions. Vision: the Journal of the Vision Society of Japan, 21(1):19–32

39. Dale, A.M., Fischl, B., and Sereno, M.I. (1999). Cortical surface-based analysis. I. Segmentation and surface reconstruction. NeuroImage *9*, 179–194.

40. Yushkevich PA, Piven J, Hazlett HC, Smith RG, Ho S, Gee JC, Gerig G. (2006). User-guided 3D active contour segmentation of anatomical structures: significantly improved efficiency and reliability. Neuroimage. 31:1116-28.

41. R Core Team (2017). R: A language and environment for statistical computing. R Foundation for Statistical Computing, Vienna, Austria. URL https://www.R-project.org/

42. Wandell, B.A., Chial, S., and Backus, B.T. (2000). Visualization and measurement of the cortical surface. Journal of cognitive neuroscience *12*, 739–752.

43. Nestares, O., and Heeger, D.J. (2000). Robust multiresolution alignment of MRI brain volumes. Magnetic Resonance in Medicine *43*, 705–715.

44. Jenkinson, M., and Smith, S. (2001). A global optimisation method for robust affine registration of brain images. Medical Image Analysis *5*, 143–156.

45. Fujita, N., Tanaka, H., Takanashi, M., Hirabuki, N., Abe, K., Yoshimura, H., and Nakamura, H. (2001). Lateral geniculate nucleus: Anatomic and functional identification by use of MR imaging. American Journal of Neuroradiology *22*, 1719–1726.

46. Dai, H., Mu, K.T., Qi, J.P., Wang, C.Y., Zhu, W.Z., Xia, L.M., Chen, Z.Q., Zhang, H., Ai, F., and Morelli, J.N. (2011). Assessment of lateral geniculate nucleus atrophy with 3T MR imaging and correlation with clinical stage of glaucoma. American Journal of Neuroradiology *32*, 1347–1353.

47. Gupta, N., Greenberg, G., De Tilly, L.N., Gray, B., Polemidiotis, M., and Yücel, Y.H. (2009). Atrophy of the lateral geniculate nucleus in human glaucoma detected by magnetic resonance imaging. British Journal of Ophthalmology *93*, 56–60.

48. Andrews, T.J., Halpern, S.D., and Purves, D. (1997). Correlated size variations in human visual cortex, lateral geniculate nucleus, and optic tract. The Journal of Neuroscience: The official journal of the Society for Neuroscience *17*, 2859–2868.